analytical chemistry

Article

pubs.acs.org/ac

Characterization of Intramolecular Interactions of Cytochrome *c* Using Hydrogen−Deuterium Exchange-Trapped Ion Mobility Spectrometry−Mass Spectrometry and Molecular Dynamics

Juan Camilo Molano-Arevalo,[†] Kevin Jeanne Dit Fouque,[†] Khoa Pham,[†] Jaroslava Miksovska,[†,‡] Mark E. Ridgeway,[§] Melvin A. Park,[§] and Francisco Fernandez-Lima*[,†,‡]

[†]Department of Chemistry and Biochemistry, Florida International University, Miami, Florida 33199, United States

[‡]Biomolecular Sciences Institute, Florida International University, Miami, Florida 33199, United States

[§]Bruker Daltonics, Inc., Billerica, Massachusetts 01821, United States

Supporting Information

ABSTRACT: Globular proteins, such as cytochrome *c* (cyt *c*), display an organized native conformation, maintained by a hydrogen bond interaction network. In the present work, the structural interrogation of kinetically trapped intermediates of cyt *c* was performed by correlating the ion-neutral collision cross section (CCS) and charge state with the starting solution conditions and time after desolvation using collision induced activation (CIA), time-resolved hydrogen/deuterium back exchange (HDX) and trapped ion mobility spectrometry−mass spectrometry (TIMS-MS). The high ion mobility resolving power of the TIMS analyzer allowed the identification of new ion mobility bands, yielding a total of 63 mobility bands over the +6 to +21 charge states and 20 mobility bands over the −5 to −10 charge states. Mobility selected HDX rates showed that for the same charge state, conformers with larger CCS present faster HDX rates in both positive and negative ion mode, suggesting that the charge sites and neighboring exchange sites on the accessible surface area define the exchange rate regardless of the charge state. Complementary molecular dynamic simulations permitted the generation of candidate structures and a mechanistic model of the folding transitions from native (N) to molten globule (MG) to kinetic intermediates (U) pathways. Our results suggest that cyt *c* major structural unfolding is associated with the distancing of the N- and C-terminal helices and subsequent solvent exposure of the hydrophobic, heme-containing cavity.

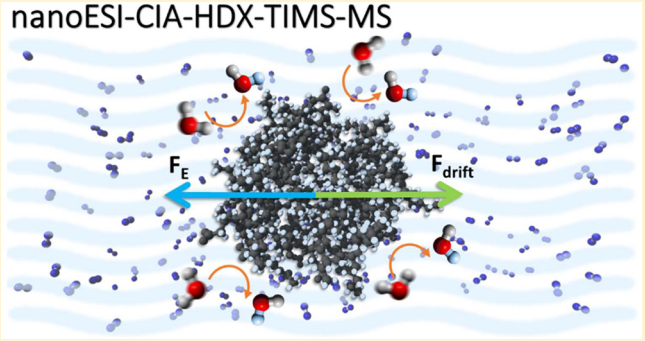

Cytochrome *c* (cyt *c*) has been widely investigated using mass spectrometry based techniques, and it has become an intriguing system for ion mobility spectrometry (IMS) and hydrogen/deuterium exchange (HDX) experiments. The appeal for IMS-based studies of cyt *c* comes from its involvement in key cellular processes,[1−4] and the interactions of the protein with multiple substrates or intracellular proteins, which in turn are associated with subtle changes in conformation. These conformational changes include fluctuations in the heme iron coordination, and tertiary and secondary structure alterations, suggesting that cyt *c* can populate different conformational states under native conditions.[5−9] With the development of soft ionization sources (e.g., electrospray ionization, ESI), the evaporative cooling of the solvent can lead to a freezing of multiple stable conformations, otherwise known as the "memory effect".[10,11] Although this effect is solvent and biomolecule dependent, previous works have reported the benefits of studying the conformational space as a function of the charge heterogeneity, the solvent conditions, as well as the transitions as a function of the bath gas collision partner and ion effective temperature.[12−16] For example, the unfolding of cyt *c*, induced with denaturing conditions, was examined by Konermann and co-workers[15] using a combination of ESI and solution-based techniques revealing that a decrease in pH induced a cooperative unfolding transition accompanied by a disruption of the secondary and tertiary structure. Mass spectra analysis, obtained as a function of the starting solution conditions, showed that the transition from low to high charge states was due to the breakdown of the tertiary structure. Early studies on cyt *c* using a drift tube, conducted by Jarrold and co-workers,[17] showed that, for the lower charge states (centered at +7, +8), the collision cross sections (CCS) of cyt *c* were consistent with those expected from native structure found in solution (PDB 1HRC, X-ray[18]). The intermediate charge states displayed metastable structures that unfolded upon heating, while the higher charge states

Received: March 7, 2017
Accepted: July 25, 2017
Published: July 25, 2017

DOI: 10.1021/acs.analchem.7b00844
Anal. Chem. 2017, 89, 8757−8765

(centered at +15, +16) exhibited CCS related to extended conformations.

Moreover, complementary structural studies were performed on cyt *c* in the gas-phase by McLafferty and co-workers[19] using a Fourier-transform ion-cyclotron-resonance mass spectrometer (FT-ICR-MS) and HDX experiments. They showed that HDX exchange of cyt *c* in the gas-phase occurs only in three different reactive forms, while in solution the reaction involves nearly all labile hydrogen atoms because of a fast dynamic equilibrium between conformers. The mass spectra of the deuterated +12 to +14 charges states exhibited peak splitting, indicating that two different ionic forms of identical molecular mass had different numbers of reactive hydrogens. These values were also observed for other charge states with 74 reactive hydrogens for the +12 to +16, 113 for the +8 to +14, and 53 for the +6 and +7 charge states. Later on, McLafferty and co-workers[20] reported at least six different states for gaseous cyt *c* ions based on their accessible sites for exchange. They also found that manipulation of these ions by infrared radiation, high velocity collisions, or proton stripping can alter the levels of exchange in discrete steps.

Using drift tube IMS experiments, Clemmer and co-workers[21] showed that it is possible to study specific conformers of cyt *c* by varying the voltage used to inject the ions into the drift tube. The number of exchangeable hydrogen atoms was independent of the charge state for diffuse conformers obtained at high injection voltages (63 of a possible 198), while the number of exchangeable hydrogens for the compact conformers, observed for the +8 to +10 charge states, was 46. These results suggested that compact structures protect some hydrogens in the gas-phase and that many sites that exchange in solution are restricted for exchange in the gas-phase, even for open conformers. Douglas and co-workers[22] investigated the conformational transitions of cyt *c* induced by denaturing conditions using HDX followed by ESI-MS and showed that the exchange rate is equal for intermediates found in both contributions of a bimodal charge state distribution. These results suggested that the intermediates are very flexible and may involve two or more rapidly interconverting conformers. They also found that at high concentrations of methanol (i.e., 90% MeOH), cyt *c* denatures into non-native helices, which protect against HDX in a similar manner to the native conformation. A later study from Douglas and co-workers[23] displayed the expanded denatured states and expanded helical denatured states of cyt *c* generated from solutions with 50% and 90% MeOH, respectively. They showed no differences in CCS and HDX for ions of a given charge state of cyt *c* for either the expanded or helical expanded denatured states. Clemmer's group later studies[24] on the HDX temperature dependence of compact (+5) and elongated (+9) cyt *c* showed that the exchange rates of HDX in the gas-phase decrease an order of magnitude when the exchange occurs at high temperature (i.e., >400 K). The exchange levels of compact (+5) and elongated (+9) conformers at 300 K were 53 and 63, respectively. At temperature values greater than 335 K, the levels increase to ∼200 for the +5 charge state and ∼190 for the +9 charge state, while the CCS remained invariant at all temperatures. Beauchamp and co-workers[25] suggested that the proximity between the charge site and exchange site are important factors in the exchange profiles of both conformers. Previous studies reported the independence between the charge states with the levels of HDX exchange in the gas-phase.[19−21,26] As noted by Clemmer and co-workers,[21] HDX numbers appear to depend strongly on the instrumentation and operating conditions used. Moreover, when CCS and HDX values are complemented with molecular dynamics (MD), candidate structures can be proposed for every kinetically trapped intermediate species observed.[27−30]

With the recent introduction of trapped ion mobility spectrometry coupled to mass spectrometry (TIMS-MS),[31−35] and more recently complemented with hydrogen/deuterium back exchange (HDX-TIMS-MS),[36] the mobility measurement and number of HDX back exchanges can be performed simultaneously as a function of time after desolvation. TIMS high resolving power (Rp up to 400)[37−39] combined with the possibility to measure kinetic intermediates and to perform collision induced activation (CIA) prior to the TIMS analysis, provides a powerful tool for the analysis of biomolecules.[40−43]

In the present work, we explore for the first time the potential of CIA-HDX-TIMS-MS to study the kinetically trapped intermediates of cyt *c* by populating the conformational free energy landscape as a function of the starting solution conditions (e.g., organic content and pH) and as a function of the CIA prior to the HDX-TIMS-MS measurements. MD simulations were used to propose candidate structures for each kinetically trapped intermediate observed and a mechanistic model of the folding transitions from native to molten globule to kinetic intermediates is proposed.

EXPERIMENTAL SECTION

Materials and Reagents. Horse heart cyt *c* (C2506) was purchased from Sigma-Aldrich (St. Louis, MO). All solvents used in these studies were analytical grade or better and purchased from Fisher Scientific (Pittsburgh, PA). Cyt *c* stock was prepared in 10 mM ammonium acetate (NH_4Ac) buffer for the positive ion mode experiments, dialyzed against the same buffer and diluted to a final concentration of 0.5, 1, 5, and 10 μM in (A) 10 mM NH_4Ac (pH 7.1), (B) 95:5 and 50:50 (v/v) H_2O/MeOH (pH 4.6), and (C) 94:5:1, 89:10:1, 79:20:1, 69:30:1, 59:40:1, and 49:50:1 H_2O/MeOH/CH_3COOH (pH 3.3). In the case of the negative ion mode analysis, a stock solution of 100 μM was used and then diluted to 40:60 (v/v) H_2O/MeOH, and 40:50:10 H_2O/TFE/Et_3N. For the HDX experiments operating in the positive ion mode, cyt *c* was prepared in D_2O (Sigma-Aldrich, 151882) at 1 μM (pH 7.02) incubated for 3 and 48 h at 37 °C and 0.1% CH_3COOH was added to solutions prior to the HDX-TIMS-MS analysis (pH 6.88). For HDX experiments operating in the negative ion mode, cyt *c* was incubated in D_2O at 50 μM. Nano-ESI emitters were pulled from quartz capillaries (O.D. = 1.0 mm and I.D. = 0.70 mm) using Sutter Instruments Co. P2000 laser puller. Low-concentration Tuning Mix calibration standard (TuneMix, G24221A) was purchased from Agilent Technologies (Santa Clara, CA).

CIA-HDX-TIMS-MS. Details regarding the TIMS operation compared to traditional IMS can be found elsewhere.[32,33,41,44,45] Briefly, TIMS mobility separation is based on holding the ions stationary using an electric field against a moving buffer gas.[46] During HDX-TIMS-MS experiments, the rate of HDX back exchange is measured as a function of the trapping time.[36] That is, in HDX-TIMS-MS deuterated, molecular ions are introduced into the TIMS cell and they can undergo back exchange reaction with residual molecules of the bath gas. The rate of HDX can be tuned by changing the velocity of the gas and the trapping time. At the end of the trapping time the ions are eluted by reducing the TIMS voltage.

DOI: 10.1021/acs.analchem.7b00844
Anal. Chem. 2017, 89, 8757−8765

The measured ion elution voltage is directly related to the ion's K as shown below.

The mobility, K, of an ion in a TIMS cell is described by

$$K = \frac{v_g}{E} = \frac{A}{(V_{elution} - V_{out})} \quad (1)$$

where v_g, E, $V_{elution}$, and V_{out} are the gas velocity, applied electric field, elution voltage, and base voltage, respectively. The constant A was determined using a Tuning Mix calibration standards (m/z 322 K_o = 1.376 $cm^2\ V^{-1}\ s^{-1}$, m/z 622 K_o = 1.013 $cm^2\ V^{-1}\ s^{-1}$, and m/z 922 K_o = 0.835 $cm^2\ V^{-1}\ s^{-1}$).[33,47]

The same RF (880 kHz and 280 Vpp) was applied to all electrodes including the entrance funnel, the ion mobility separating section, and the exit funnel (Figure S1). A custom-made nanoelectrospray ionization source was used for all the analyses. TIMS separation was performed using nitrogen as a bath gas at 300 K, and the gas flow velocity was held constant in all the experiments (P_1 = 2.6 and P_2 = 1.0 mbar). P_1 and P_2 values were held constant for all experiments. A fill/trap/ramp/wait sequence of 1−10/1−10/5−500/50 ms was used and an average mobility resolution of 180−250 was observed. A total of 500 accumulations and 10 frames were acquired per TIMS experiment.

Mobility values (K) were correlated with CCS (Ω, $Å^2$) using the following equation

$$\Omega = \frac{(18\pi)^{1/2}}{16}\frac{z}{(k_B T)^{1/2}}\left(\frac{1}{m_I} + \frac{1}{m_b}\right)^{1/2}\frac{1}{K}\frac{760}{P}\frac{T}{273.15}\frac{1}{N^*} \quad (2)$$

where z is the charge of the ion, k_B is the Boltzmann constant, N^* is the number density, and m_I and m_b refer to the masses of the ion and bath gas, respectively.[46]

The number of HDX back-exchanges is obtained by the mass shift relative to the nondeuterated protein (Figure S2). Collision induced activation was performed prior to the TIMS-MS by varying the electric field between the capillary outlet (V_{cap} = 50−190 V), deflector plate (V_{def} = 60−200 V) and funnel entrance (V_{fun} = 0−150 V) in 10 V steps.

Theoretical Method. A candidate structure generation algorithm was used to sample cyt *c* conformational space.[48] The 1HRC protein data bank entry for cyt *c* was utilized as the starting structure.[18,49] Briefly, molecular dynamics simulations were used to reproduce the experimental conditions and to generate the identity vectors that define cyt *c* conformational space. This approach is similar to that previously described by Fernández-Lima et al.[13] for peptides, with the main characteristic that the initial search targets the generation of the identity vectors, followed by charge assignment and energy minimization. Once the candidate structures were identified for each IMS band, charge assignment was performed by scoring the accessible surface area based on the score of the amino acid residues.[50,51] For example, solvent accessibility and the pK_a of the acidic and basic residues were primarily used to assign the protonation and deprotonation sites. It is known that charge localization can influence electrostatic interactions and therefore the conformational dynamics of molecular ions.[52,53] To account for the charge state influence on the CCS, energy optimization steps were performed following the charge assignments. All simulations were performed in a NVT thermostat using AMBER03 force field in YASARA software. The molecular dynamic simulations yielded identity vectors that cover the +6 to +13 distributions and the theoretical CCS_{N2} for each structure were calculated using the TM algorithm implemented in the iMoS software.[54−56]

RESULTS AND DISCUSSION

The mass spectrometry analysis of cyt *c* in positive and negative ion mode displayed a charge state distribution dependence with the solvent conditions in agreement with previous studies.[15,22] Under native conditions (e.g., 0% MeOH, 10 mM NH_4Ac), a narrow distribution of charge states centered at +7 was observed (Figure 1, left panel on the top). An increase in the concentration of MeOH to 5% showed a conformational change in the protein, represented by a bimodal distribution with two envelopes centered at +9 and +17. Further increases in the concentration of MeOH decreased the relative intensity of the envelope for the lower native-like charge states (e.g., + 6 to +9) and a single distribution was observed at 40% MeOH centered at +17. For the negative ion mode, the −5 and −6 charge states were observed for a solution with 40% MeOH (Figure 1, left panel on the bottom). A change in the starting solvent condition using 50% TFE and 10% Et_3N showed a conformational change in the cyt *c* represented by a different charge state distribution centered at −8. To confirm the conformational diversity of cyt *c* under different solution conditions, ultraviolet−visible (UV−vis) spectroscopy was used to trace the Soret band intensity to monitor the accessibility of solvent to the heme group as the band shifts from 400 to 395 nm after acidification of the solution (Figure S3). As previously described by Konermann et al.,[15] in aqueous solutions of low ionic strength, cyt *c* is in the native state and the heme iron is coordinated by the strong-field ligands His18 and Met80 residues, which produces a low spin complex with a Soret absorption maximum between 400 and 410 nm.[18,57−61] Further acidification of the solution or an increase in the MeOH

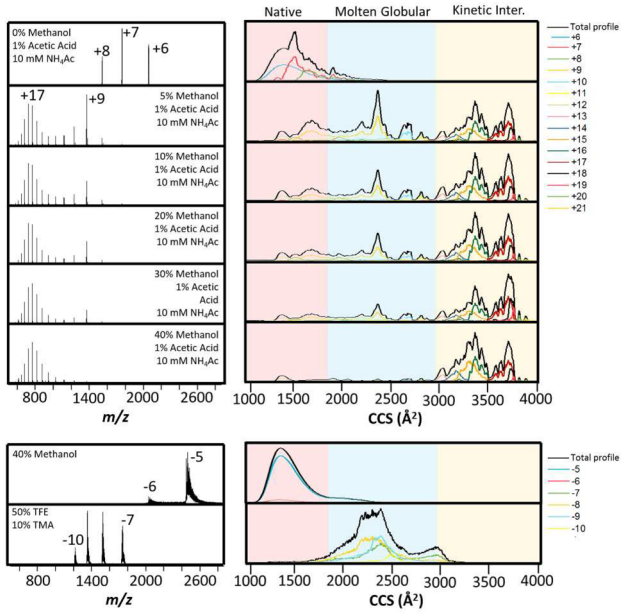

Figure 1. Left panel: Typical mass spectra of cyt *c* as a function of the starting solvent conditions. Right panel: Overall CCS profiles (black lines) obtained by summation of the intensity-normalized IMS resolved data (color lines). The results obtained in the positive and negative ion mode are represented on the top and bottom part, respectively.

DOI: 10.1021/acs.analchem.7b00844
Anal. Chem. 2017, 89, 8757−8765

concentration induces a cooperative unfolding transition to a molten-globule state,[60,62,63] and the displacement of both strong-field ligands by weak-field ligands from the solvent (e.g., H_2O) produces a high-spin complex with a Soret absorption between 390 and 395 nm.[59,60,64]

IMS profiles for the observed charge states on each condition were normalized to the intensity of each charge state in the mass spectrum (Figure 1, right panel). The overall CCS profiles (Figure 1, black lines) obtained by summation of the ion mobility resolved data (Figure 1, color lines), exhibited a distribution of conformations from native (Figure 1, red background) to molten globular (Figure 1, blue background), and finally to the denatured states trapped as kinetic intermediates (Figure 1, yellow background). Ion mobility experiments were performed as a function of the starting solution conditions and the collision induced activation (CIA) energy (Figure 2) in the positive ion mode. Soft activation

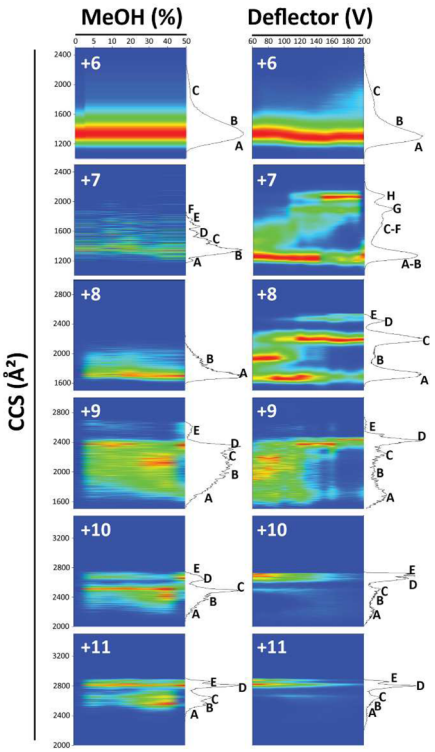

Figure 2. Left panel: IMS spectra of the +6 to +11 charges states of cyt *c* as a function of the organic content (e.g., % methanol). Right panel: IMS spectra of the +6 to +11 charge states of cyt *c* as a function of the activation energy (e.g., deflector voltage).

energy conditions were used to preserve the conformation from the solution (e.g., V_{cap} = 50 V, V_{def} = 60 V, and V_{fun} = 0 V). In addition, TIMS analyzers permit the study of the temporal evolution of the IMS distribution as a function of the time after the molecular ions are formed during the nanoESI process (e.g., trapping time of 100−500 ms after desolvation). Inspection of the IMS bands as a function of the trapping time did not show variation in terms of the relative abundance. However, previous reports have shown variation of the IMS profiles of cyt *c* at shorter times after desolvation.[29] This result suggests that the observed IMS bands in TIMS correspond to stable "desolvated", kinetically trapped intermediates. As displayed in the mass spectrometry analysis, the IMS profiles for the +8 to +11 charge states are obtained when the starting solution contains at least 5% MeOH, suggesting that a solution only with 10 mM NH_4Ac cannot induce the necessary conformational changes that allows basic sites to be protonated during the nanoESI process. The overall IMS profiles for all the solution conditions are shown next to the contour plots, where IMS bands are labeled for the kinetically trapped intermediates (Figure 2, left panel). Most IMS profiles are uniform as a function of the starting solution conditions. Interestingly, the contour plot for the +9 charge state is broad and displays heterogeneity in the relative intensity of B and C, whereas a variation in their relative abundance is observed after the addition of 20% MeOH to the solution (Figure 2, left panel). We interpret this result as evidence of kinetic intermediates involved in the transition from native-like to molten globular conformation. In a similar way, the IMS profiles for the +10, label B, and +11, labels B and C, charge states are more intense when the solution contains 30% and 20% MeOH, respectively.

Another way to probe the conformational space of cyt *c* in the gas phase is to activate the ions prior to IMS analysis (Figure 2, right panel). Note that the label in the CIA plots only shows the deflector voltage (V_{def}) as the variable, but the voltage of the both capillary (V_{cap}) and entrance funnel (V_{fun}) regions were increased accordingly using 10 V increments per experiment. The solution used for these experiments was 10 μM of cyt *c* in 10 mM NH_4Ac, 5% MeOH, and 1% CH_3COOH. Examination of the contour plots exhibited little variation in the IMS profiles for the +6, +10, and +11 charge states as a function of the activation energy (Figure 2, right panel). It is possible that the energy used to activate the ions is not enough to disrupt the intramolecular interactions from the hydrogen bond network that holds together the compact native-like conformations observed in the +6 charge state. The conformations for the +10 and +11 charge states are already open, and the additional energy does little to populate more extended structures. However, it is interesting to note the changes in the intensity of the IMS bands (labels D and E) for the +10 charge state relative to the solution obtained profile, suggesting that, even though all the conformers are observed, the open conformations are more stable and abundant when the activation takes place. Inspection of the contour plot for the +7 charge state showed a broad band, which combines the compact conformers A and B (Figure 2, right panel). A stepwise transition between conformations C through F end in the trapping of two new open conformers (labels G and H) when the CIA energy is high (i.e., V_{cap} = 130 V, V_{def} = 140 V, and V_{fun} = 80 V). The IMS profile for the +8 charge state showed the trapped intermediates observed in solution (labels A and B) and two generated as the CIA energy increases and the trapped intermediates are allowed to climb the energy funnel barriers and populate different local minima (i.e., labels C and D at V_{cap} = 80 V, V_{def} = 90 V, V_{fun} = 30 V and label E at V_{cap} = 140 V, V_{def} = 150 V, V_{fun} = 90 V). The IMS profile for the +9 charge state also displays a broad transition between conformers as the solution conditions changes (Figure 2, right panel). However, when the ions are activated, it is possible to better distinguish the A, B, and C IMS bands. These results for the +7, + 8, and +9 charge states show that the transition between compact and open conformers can be induced via CIA. That is, when the internal energy of the protein increases and overcomes the conformational energy barrier, other local minima are accessible. The CCS and K_0 values are summarized in Table S1.

DOI: 10.1021/acs.analchem.7b00844
Anal. Chem. 2017, 89, 8757−8765

The high IMS resolving power of the TIMS analyzer allowed to observe a larger number of IMS bands than those observed in previous works for charge states higher than +11 (Figure 3 and Table S2). Moreover, inspection of the +12 to +21 charge states exhibited a reduction in the number of IMS bands and narrower distributions when compared to the +8 to +11 charge states. No major differences are found in the IMS profiles for the +12 to +21 charge states as a function of the solution conditions, the activation energy, or the trapping time. Nevertheless, when compared to previous IMS experiments a larger number of IMS bands are now separated using TIMS for the +12 to +21 charge states. Complementary TIMS experiments with varying cyt c concentration (e.g., 0.5, 1, 5, and 10 μM) rule out the possibility of IMS bands corresponding to the formation of multimeric assemblies. The TIMS data are consistent with previous CCS reports on cyt *c* using other IMS variants (Figure S4).

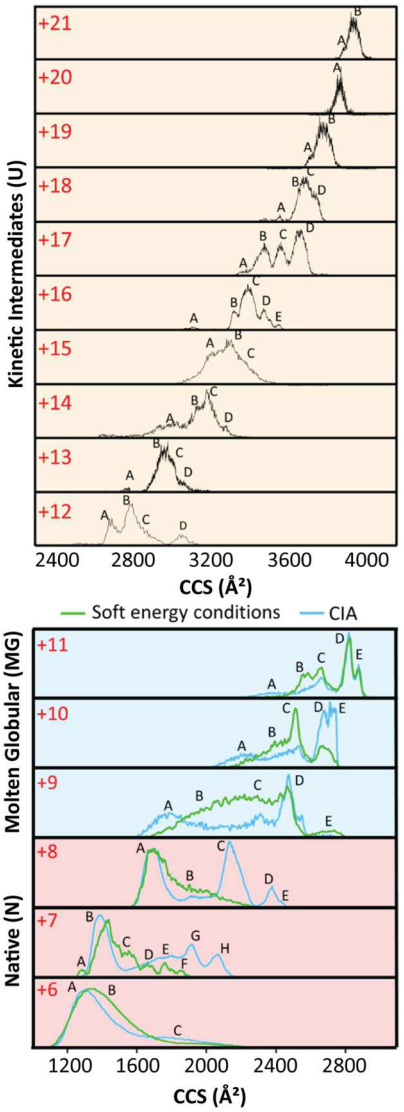

Figure 3. Bottom: IMS profiles obtained with CIA (blue line), and without CIA (green line). Top: High resolution IMS profiles for the +12 to +21 charge states of cyt *c*.

This discussion can be followed by the inspection of the cyt *c* back-exchange HDX dynamics in the TIMS analyzer (Figure 4). Two HDX incubation time were considered, 3 and 48 h in D_2O, followed by 50 ms TIMS measurement intervals (Figure S5). IMS resolved HDX data were acquired for all the IMS bands of the +6 to +13 charge states. In solution, at physiological conditions (e.g., 37 °C, pH 7.0), most molecules of cyt *c* are probably populating the "native" state conformations (lower minima of the free energy landscape). Local unfolding events in an excess of D_2O allow the exchange reaction between amide hydrogens and deuterons by any of the three well-known mechanisms (i.e., base catalysis, acid catalysis by N-protonation, and acid catalysis by O-protonation).[65−68] During the nanoESI process, the cyt c molecules are protonated in positive ion mode as a function of the degree of exposure of basic residues. If a low amount of acid is added to the solution, the conformation of some of the protein molecules is disturbed from the native state, allowing the fast exchange of usually slow-exchanging hydrogens. Our results showed independence between the initial number of deuterons and the charge state for all the incubation conditions, and the number of initial deuterons was never close to the maximum number of possible exchanges (i.e., 196). For example, HDX-TIMS analysis without trapping (t_{trap} = 0 ms) and with back-exchange trapping (t_{trap} = 100−500 ms) showed that the number of deuterons is independent from the charge state for the two incubation times considered (Figure 4). The initial number of deuterons at 48 h is considerably higher than at 3 h, as many of the nonexposed hydrogen atoms involved in the hydrogen bond network that preserves the protein structure may have exchanged during incubation, most likely due to conformational rearrangements and small movements that expose these otherwise protected atoms. To generate ions of higher charge states, a small amount of acid (i.e., 0.1% CH_3COOH) was added to the incubated solutions (pH 6.88). It is possible that the addition of a small amount of acid might be enough to quench, at least in some degree, the exchange reaction between the exposed slow-exchanging hydrogens and the deuterons from the solvent, or, as the quenching is not complete, some

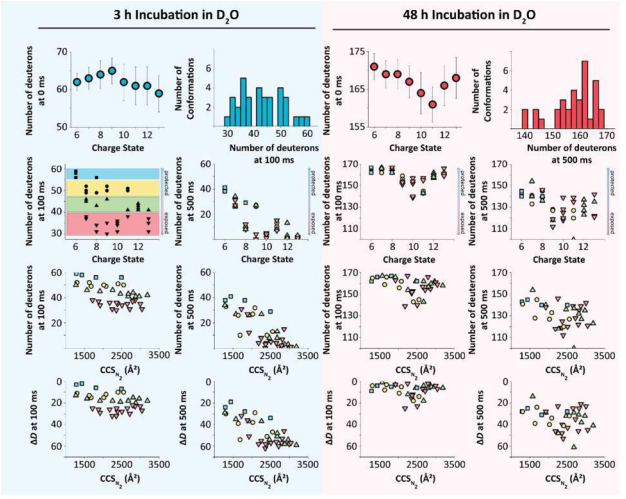

Figure 4. HDX back exchange as a function of the incubation time (e.g., 3 and 48 h) and the time after desolvation (e.g., 0, 100, and 500 ms), in terms of charge state and CCS in the positive ion mode. Clustering of the number of kinetically trapped intermediates and the initial levels of exchange allows the identification of four groups with different levels of exchange protection (color rectangles and data points).

DOI: 10.1021/acs.analchem.7b00844
Anal. Chem. 2017, 89, 8757−8765

exchange still occurs when the protein unfolds due the denaturing effect of the acid, which leads to a slight overestimation of the number of initial deuterons for the higher charge states. However, the range of HDX-TIMS back-exchange after 100 ms is narrower at 48 h compared to 3 h; this result suggests that some hydrogen atoms can slowly exchange in solution but they are not readily accessible for back-exchange in the gas-phase. Clustering of the number of conformations based on the number of deuterons at t_{trap} = 100 ms revealed four major conformational groups (Figure 4), which can be associated with different levels of protection (Figure S6). A small shortcoming of the current experimental setup is that the residual water content in the TIMS cell is not controlled or monitored, leading to potential differences in the total number of exchanges between experiments due to samples with different water/D_2O content and spraying conditions (example Figure 4, ΔD for 3h and 48h of incubation). Most importantly, it does not alter the features observed within a single experiment (e.g., same infusion) where most of the benefit of HDX-TIMS technique relies (e.g., direct comparison of the exchange levels between charge states and mobility bands). The HDX-TIMS back-exchange follows a general declining trend (Figure S5). For some cases (e.g., + 13 charge state) a bimodal distribution is observed, where a fast back exchange occurs within the first 200 ms. Since changes are not observed in the CCS distribution over the trapping time, we interpret the bimodal distribution as a consequence of similar conformations with different charge configuration, and to a lesser extend to minor conformational rearrangements exposing more hydrogens that are not resolved in the CCS domain.

Traditional HDX experiments use the relay-mechanism to explain the isotopic exchange in the gas-phase via charge-mediated exchanges in a timely efficient manner[69−72] The HDX-TIMS experiments share some analogy with thermal energy HDX ion−molecule reactions used to probe conformational differences by Smith and co-workers,[73] but HDX-TIMS back-exchange ion-neutral reactions are performed at lower pressures (few mbar), larger free mean path, and low energy transfer per collision. The HDX-TIMS back-exchange relies on collisions of the kinetically trapped intermediates with residual water molecules, which can be experimentally tailored by the velocity of the gas or by the amount of residual water in the system. Closer inspection to the back-exchange rates for a given charge state, in both positive and negative ion mode, showed that as the CCS increases, faster HDX rates are observed (Figure 4 and Tables S1 and S3). Moreover, similar rates are observed for conformers of the same conformational state (e.g., N or MG) regardless of the charge state or polarity (Figure S7). We interpret these results as a consequence of the accessible surface area per conformational state. That is, there are regions on the surface of the protein that allow for the back HDX to occur, probably determined by the charge sites and distance to the exchange sites as previously suggested by Beauchamp and co-workers.[25] For example, differences in back HDX rates with the CCS per charge state can be related to different charge configurations, which based on the position of the charge site and neighboring amino acids will ultimately define the HDX rate. Notice that HDX-TIMS experiments are particularly suitable for the study of cyt c accessible surface area during its unfolding pathway. Exposed deuterons back-exchange faster while buried deuterons are protected, providing a better insight into the structural dynamics of cyt c unfolding. While this initial set of experiments only give a qualitative view of the hydrogen network, charge configuration, and the CCS of the cyt c kinetic intermediates, further experiments using top-down strategies on mobility selected HDX time points will permit further assessment of the intramolecular forces that stabilize the cyt c kinetic intermediates.

Candidate structures were proposed for all IMS bands (Figure 5). Closer inspection to the candidate structures

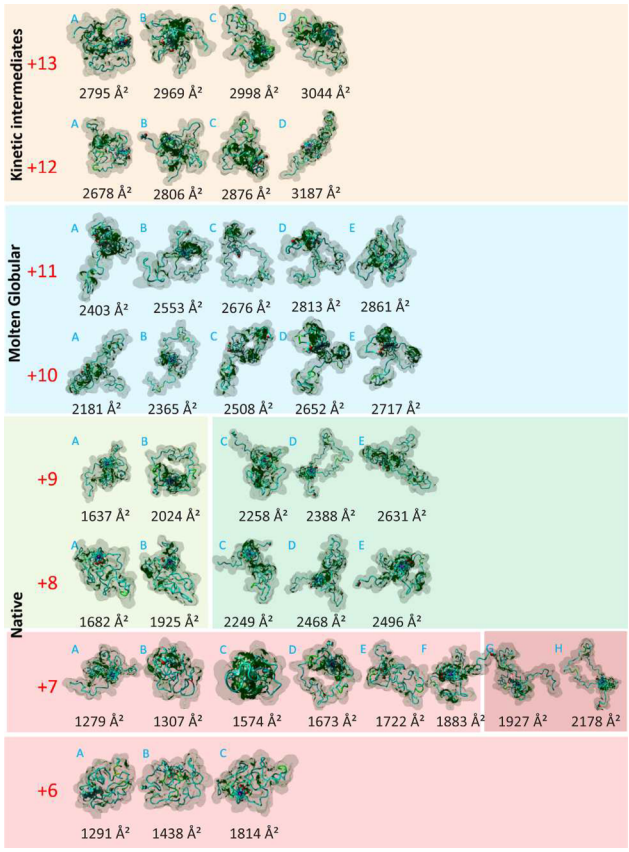

Figure 5. Candidate structures proposed for the kinetic intermediates IMS bands of cyt *c*. Conformations G and H for the +7 charge state (dark red background); and C, D, and E (dark green background), for the +8, and +9 charge states, were obtained after CIA.

permitted the generation of a mechanistic model of the main intramolecular interactions that define the folding pathways and their intermediates (Figure S8). For example, inspection of the candidate structures revealed that major structural differences are associated with the increase in distance between the N- and C- terminal helices and the solvent exposure of the heme cavity at higher charge states are consistent with previous results.[74−76] That is, the +10 charge state structures are characterized by the destabilization of the secondary structure of the N- and C-terminal helices and cleavage of the Trp59 and of the Met80 residues and the heme propionate hydrogen bond. It has been reported that Trp59 and Met80 residues provide a unique hydrophobic environment to the heme crevice.[77,78] Without these interactions, the crevice opens up, exposing Thr78 and Pro71, which are residues involved in the formation and stabilization of the heme crevice due a network of hydrogen bonds around the heme group.[79] The interface formed by the interaction of the helices occurs immediately after the covalent binding of the heme group to the polypeptide via thioether bonds.[80] Closer inspection of the candidate structures for the

DOI: 10.1021/acs.analchem.7b00844
Anal. Chem. 2017, 89, 8757−8765

+6, + 7, and +8 charge states revealed that the $\pi-\pi$ interaction of Phe10 and Tyr97 aromatic groups is lost followed by the loss of the "peg-in-a-hole" Gly6 and Leu94 interaction, which is also consistent with previous observations.[81] For example, the +8 charge state of cyt *c* showed that Gly6 and Leu94 residues are interacting while there is a distancing between Phe10 and Tyr97 residues compared to the structures generated for the +6 and +7 charge states. Moreover, structures for the +8 charge state displayed an increasing separation between the N- and C-terminal helices while conserving the interaction between Gly6 and Leu94 residues. The +9 charge state of cyt *c* showed that Gly6 residue is no longer interacting with Leu94 residue, and the +9 conformations exhibited a widening gap between these two amino acids while conserving the general structure of the N- and C- terminal helices. It should be noted that when compared to the myoglobin folding/unfolding pathway,[36] the covalent attachment of the heme in cyt *c* stabilizes the MG and U intermediate states (less structural flexibility) into more defined IMS bands.

CONCLUSIONS

The high mobility resolving power of the TIMS analyzer allowed the identification of new ion mobility bands for cyt c, yielding a total of 63 mobility bands over the +6 to +21 charge states and 20 mobility bands over the −5 to −10 charge states. Experimental results showed that only 5% methanol and 1% acetic acid can disrupt the intramolecular interactions (i.e., hydrogen bond network) that holds together the integrity of the native conformation. TIMS-MS experiments enabled us to establish a general trend where the trapped intermediates increase in CCS as a function of the charge state and the inspection of the candidate structures proposed for the lower charge states (i.e., + 6 and +7, and −5 and −6) confirmed that the solution "native" states are retained in the gas-phase. For the first time using a TIMS analyzer, we describe how the collisional activation of the desolvated ions permitted the generation of other conformational states of cyt *c* that are not readily accessible by varying the starting solution. Our results suggest that major structural unfolding motifs were associated with the distance between the N- and C-terminal helices and the solvent exposure of the heme cavity.

The possibility of measuring CCS and HDX back-exchange rates simultaneously, permitted the identification of local fluctuations which might later be useful in the identification of features that define the structure of cyt c kinetically trapped intermediates. The hydrogens exposed in the surface of the protein, which can be partially involved (or not) in the hydrogen bond interaction network, are readily exchangeable. The effect of the rearrangement of the contact points between secondary structures, which disrupts the hydrogen bond interaction network but keep the overall integrity of the protein, allows the identification of the number of hydrogens completely buried that are not going to exchange because of their role preserving the native conformation of the protein. In the case of cyt *c*, changes in the HDX rates were observed as a function of the CCS for the same charge state, which can be related to different charge configurations. In particular, for the first-time experimental evidence based on HDX-TIMS is provided that support the idea of microheterogeneity during HDX as previously suggested by Beauchamp and co-workers,[25] where the charge sites and neighboring exchange sites on the accessible surface area of the protein define the exchange rate regardless of the molecular ion charge state.

The HDX-TIMS-MS experiments provide a powerful analytical tool for the study of protein folding and intermediates. While major advances are highlighted in the present case, further improvements by performing top-down experiments in HDX-TIMS selected intermediates will provide a more detailed description on the charge configuration for more accurate candidate structure generation.

ASSOCIATED CONTENT

Supporting Information

The Supporting Information is available free of charge on the ACS Publications website at DOI: 10.1021/acs.analchem.7b00844.

Scheme of the TIMS cell, experimental and theoretical mass shift for the deuterated and nondeuterated +6 and +13 charge states, UV−vis spectroscopy in the 300−600 nm spectral range of cyt *c*, summary of CCS literature values for cyt *c*, number of exchanges as a function of the trapping time and the incubation time with and without CIA, clustering of HDX protection groups based on the number of deuterons and the number of conformations, number of exchanges as a function of the trapping time in the negative ion mode, unfolding pathway of cyt *c*, experimental results of HDX as a function of the incubation time and CCS of cyt *c* for the +6 to +13 charge states, and experimental CCS of cyt *c* for the +14 to +21 and −5 to −10 charge states. (PDF)

AUTHOR INFORMATION

Corresponding Author

*E-mail: fernandf@fiu.edu.

ORCID

Jaroslava Miksovska: 0000-0002-0385-9457

Francisco Fernandez-Lima: 0000-0002-1283-4390

Author Contributions

The manuscript was written through contributions of all authors, and all authors have given approval to the final version of the manuscript.

Funding

The authors acknowledge the financial support from the National Institute of Health (R00GM106414), a Bruker Daltonics Inc. fellowship, and the National Science Foundation Division of Chemistry, under CAREER award CHE-1654274, with cofunding from the Division of Molecular and Cellular Biosciences to FFL.

Notes

The authors declare no competing financial interest.

ACKNOWLEDGMENTS

The authors would like to acknowledge the Instructional & Research Computing Center (IRCC) at Florida International University for providing high performance computing resources that have contributed to the results reported within this research.

REFERENCES

(1) Huttemann, M.; Pecina, P.; Rainbolt, M.; Sanderson, T. H.; Kagan, V. E.; Samavati, L.; Doan, J. W.; Lee, I. *Mitochondrion* **2011**, *11*, 369−381.

(2) Liu, X.; Kim, C. N.; Yang, J.; Jemmerson, R.; Wang, X. *Cell* **1996**, *86*, 147−157.

DOI: 10.1021/acs.analchem.7b00844
Anal. Chem. 2017, 89, 8757−8765

(3) Pereverzev, M. O.; Vygodina, T. V.; Konstantinov, A. A.; Skulachev, V. P. *Biochem. Soc. Trans.* **2003**, *31*, 1312−1315.
(4) Kagan, V. E.; Borisenko, G. G.; Tyurina, Y. Y.; Tyurin, V. A.; Jiang, J.; Potapovich, A. I.; Kini, V.; Amoscato, A. A.; Fujii, Y. *Free Radical Biol. Med.* **2004**, *37*, 1963−1985.
(5) Stevens, J. M. *Metallomics* **2011**, *3*, 319−322.
(6) Yeh, S. R.; Rousseau, D. L. *Nat. Struct. Biol.* **1998**, *5*, 222−228.
(7) Tezcan, F. A.; Findley, W. M.; Crane, B. R.; Ross, S. A.; Lyubovitsky, J. G.; Gray, H. B.; Winkler, J. R. *Proc. Natl. Acad. Sci. U. S. A.* **2002**, *99*, 8626−8630.
(8) Smith, L. J.; Kahraman, A.; Thornton, J. M. *Proteins: Struct., Funct., Genet.* **2010**, *78*, 2349−2368.
(9) Sauder, J. M.; Roder, H. *Folding Des.* **1998**, *3*, 293−301.
(10) Li, J.; Taraszka, J. A.; Counterman, A. E.; Clemmer, D. E. *Int. J. Mass Spectrom.* **1999**, *185*−*187*, 37−47.
(11) Wang, F.; Freitas, M. A.; Marshall, A. G.; Sykes, B. D. *Int. J. Mass Spectrom.* **1999**, *192*, 319−325.
(12) Wyttenbach, T.; von Helden, G.; Bowers, M. T. *J. Am. Chem. Soc.* **1996**, *118*, 8355−8364.
(13) Fernandez-Lima, F. A.; Wei, H.; Gao, Y. Q.; Russell, D. H. *J. Phys. Chem. A* **2009**, *113*, 8221−8234.
(14) Zhong, Y.; Hyung, S. J.; Ruotolo, B. T. *Expert Rev. Proteomics* **2012**, *9*, 47−58.
(15) Konermann, L.; Douglas, D. J. *Biochemistry* **1997**, *36*, 12296−12302.
(16) Shvartsburg, A. A. *Anal. Chem.* **2014**, *86*, 10608−10615.
(17) Shelimov, K. B.; Clemmer, D. E.; Hudgins, R. R.; Jarrold, M. F. *J. Am. Chem. Soc.* **1997**, *119*, 2240−2248.
(18) Bushnell, G. W.; Louie, G. V.; Brayer, G. D. *J. Mol. Biol.* **1990**, *214*, 585−595.
(19) Suckau, D.; Shi, Y.; Beu, S. C.; Senko, M. W.; Quinn, J. P.; Wampler, F. M., 3rd; McLafferty, F. W. *Proc. Natl. Acad. Sci. U. S. A.* **1993**, *90*, 790−793.
(20) Wood, T. D.; Chorush, R. A.; Wampler, F. M., 3rd; Little, D. P.; O'Connor, P. B.; McLafferty, F. W. *Proc. Natl. Acad. Sci. U. S. A.* **1995**, *92*, 2451−2454.
(21) Valentine, S. J.; Clemmer, D. E. *J. Am. Chem. Soc.* **1997**, *119*, 3558−3566.
(22) Babu, K. R.; Moradian, A.; Douglas, D. J. *J. Am. Soc. Mass Spectrom.* **2001**, *12*, 317−328.
(23) Wright, P. J.; Zhang, J.; Douglas, D. J. *J. Am. Soc. Mass Spectrom.* **2008**, *19*, 1906−1913.
(24) Valentine, S. J.; Clemmer, D. E. *J. Am. Soc. Mass Spectrom.* **2002**, *13*, 506−517.
(25) Campbell, S.; Rodgers, M. T.; Marzluff, E. M.; Beauchamp, J. L. *J. Am. Chem. Soc.* **1995**, *117*, 12840−12854.
(26) McLafferty, F. W.; Guan, Z. Q.; Haupts, U.; Wood, T. D.; Kelleher, N. L. *J. Am. Chem. Soc.* **1998**, *120*, 4732−4740.
(27) Fenn, J. B.; Mann, M.; Meng, C. K.; Wong, S. F.; Whitehouse, C. M. *Science* **1989**, *246*, 64−71.
(28) Clemmer, D. E.; Hudgins, R. R.; Jarrold, M. F. *J. Am. Chem. Soc.* **1995**, *117*, 10141−10142.
(29) Badman, E. R.; Hoaglund-Hyzer, C. S.; Clemmer, D. E. *Anal. Chem.* **2001**, *73*, 6000−6007.
(30) Dickinson, E. R.; Jurneczko, E.; Pacholarz, K. J.; Clarke, D. J.; Reeves, M.; Ball, K. L.; Hupp, T.; Campopiano, D.; Nikolova, P. V.; Barran, P. E. *Anal. Chem.* **2015**, *87*, 3231−3238.
(31) Fernandez-Lima, F.; Blase, R. C.; Russell, D. H. *Int. J. Mass Spectrom.* **2010**, *298*, 111−118.
(32) Fernandez-Lima, F.; Kaplan, D. A.; Suetering, J.; Park, M. A. *Int. J. Ion Mobility Spectrom.* **2011**, *14*, 93−98.
(33) Hernandez, D. R.; Debord, J. D.; Ridgeway, M. E.; Kaplan, D. A.; Park, M. A.; Fernandez-Lima, F. *Analyst* **2014**, *139*, 1913−1921.
(34) Fernandez-Lima, F. *Int. J. Ion Mobility Spectrom.* **2016**, *19*, 65−67.
(35) Benigni, P.; Fernandez-Lima, F. *Anal. Chem.* **2016**, *88*, 7404−7412.
(36) Schenk, E. R.; Almeida, R.; Miksovska, J.; Ridgeway, M. E.; Park, M. A.; Fernandez-Lima, F. *J. Am. Soc. Mass Spectrom.* **2015**, *26*, 555−563.
(37) Ridgeway, M. E.; Silveira, J. A.; Meier, J. E.; Park, M. A. *Analyst* **2015**, *140*, 6964−6972.
(38) Silveira, J. A.; Ridgeway, M. E.; Park, M. A. *Anal. Chem.* **2014**, *86*, 5624−5627.
(39) Adams, K. J.; Montero, D.; Aga, D.; Fernandez-Lima, F. *Int. J. Ion Mobility Spectrom.* **2016**, *19*, 69−76.
(40) Schenk, E. R.; Mendez, V.; Landrum, J. T.; Ridgeway, M. E.; Park, M. A.; Fernandez-Lima, F. *Anal. Chem.* **2014**, *86*, 2019−2024.
(41) Schenk, E. R.; Ridgeway, M. E.; Park, M. A.; Leng, F.; Fernandez-Lima, F. *Anal. Chem.* **2014**, *86*, 1210−1214.
(42) Garabedian, A.; Butcher, D.; Lippens, J. L.; Miksovska, J.; Chapagain, P.; Fabris, D.; Ridgeway, M. E.; Park, M. A.; Fernandez-Lima, F. *Phys. Chem. Chem. Phys.* **2016**, *18*, 26691−26702.
(43) Pu, Y.; Ridgeway, M. E.; Glaskin, R. S.; Park, M. A.; Costello, C. E.; Lin, C. *Anal. Chem.* **2016**, *88*, 3440−3443.
(44) Fernandez-Lima, F. A.; Kaplan, D. A.; Park, M. A. *Rev. Sci. Instrum.* **2011**, *82*, 126106.
(45) Molano-Arevalo, J. C.; Hernandez, D. R.; Gonzalez, W. G.; Miksovska, J.; Ridgeway, M. E.; Park, M. A.; Fernandez-Lima, F. *Anal. Chem.* **2014**, *86*, 10223−10230.
(46) McDaniel, E. W.; Mason, E. A. *Mobility and Diffusion of Ions in Gases*; John Wiley and Sons, Inc.: New York, 1973; p 381.
(47) Flanagan, L. A. (Hewlett-Packard Company, Palo Alto, CA) U.S. Patent No. 5872357 A, February 16, 1999.
(48) Schenk, E. R.; Nau, F.; Fernandez-Lima, F. *Int. J. Ion Mobility Spectrom.* **2015**, *18*, 23−29.
(49) Evans, S. V.; Brayer, G. D. *J. Mol. Biol.* **1990**, *213*, 885−897.
(50) Bogatyreva, N. S.; Ivankov, D. N. *Mol. Biol.* **2008**, *42*, 932−938.
(51) Kaltashov, I. A.; Mohimen, A. *Anal. Chem.* **2005**, *77*, 5370−5379.
(52) Susa, A. C.; Mortensen, D. N.; Williams, E. R. *J. Am. Soc. Mass Spectrom.* **2014**, *25*, 918−927.
(53) Onufriev, A.; Case, D. A.; Bashford, D. *J. Mol. Biol.* **2003**, *325*, 555−567.
(54) Larriba, C.; Hogan, C. J., Jr. *J. Phys. Chem. A* **2013**, *117*, 3887−3901.
(55) Larriba, C.; Hogan, C. J. *J. Comput. Phys.* **2013**, *251*, 344−363.
(56) Shrivastav, V.; Nahin, M.; Hogan, C. J.; Larriba-Andaluz, C. *J. Am. Soc. Mass Spectrom.* **2017**, *28*, 1540−1551.
(57) Stellwagen, E.; Rysavy, R.; Babul, G. *J. Biol. Chem.* **1972**, *247*, 8074−8077.
(58) Stellwagen, E.; Babul, J. *Biochemistry* **1975**, *14*, 5135−5140.
(59) Drew, H. R.; Dickerson, R. E. *J. Biol. Chem.* **1978**, *253*, 8420−8427.
(60) Babul, J.; Stellwagen, E. *Biochemistry* **1972**, *11*, 1195−1200.
(61) Babul, J.; Stellwagen, E. *Biopolymers* **1971**, *10*, 2359−2361.
(62) Knapp, J. A.; Pace, C. N. *Biochemistry* **1974**, *13*, 1289−1294.
(63) Theorell, H.; Åkesson, Å. *J. Am. Chem. Soc.* **1941**, *63*, 1804−1811.
(64) Robinson, J. B., Jr.; Strottmann, J. M.; Stellwagen, E. *J. Biol. Chem.* **1983**, *258*, 6772−6776.
(65) Perrin, C. L. *Acc. Chem. Res.* **1989**, *22*, 268−275.
(66) Englander, S. W.; Kallenbach, N. R. *Q. Rev. Biophys.* **1983**, *16*, 521−655.
(67) Englander, S. W.; Downer, N. W.; Teitelbaum, H. *Annu. Rev. Biochem.* **1972**, *41*, 903−924.
(68) Berger, A.; Loewenstein, A.; Meiboom, S. *J. Am. Chem. Soc.* **1959**, *81*, 62−67.
(69) Campbell, S.; Rodgers, M. T.; Marzluff, E. M.; Beauchamp, J. L. *J. Am. Chem. Soc.* **1995**, *117*, 12840−12854.
(70) Tüchsen, E.; Woodward, C. *J. Mol. Biol.* **1985**, *185*, 405−419.
(71) Tüchsen, E.; Woodward, C. *J. Mol. Biol.* **1985**, *185*, 421−430.
(72) Lioe, H.; O'Hair, R. A.; Reid, G. E. *J. Am. Soc. Mass Spectrom.* **2004**, *15*, 65−76.
(73) Winger, B.; Light-Wahl, K.; Rockwood, A.; Smith, R. D. *J. Am. Chem. Soc.* **1992**, *114*, 5897−5898.

DOI: 10.1021/acs.analchem.7b00844
Anal. Chem. 2017, 89, 8757−8765

(74) Roder, H.; Elove, G. A.; Englander, S. W. *Nature* **1988**, *335*, 700−704.
(75) Fumo, G.; Spitzer, J. S.; Fetrow, J. S. *Gene* **1995**, *164*, 33−39.
(76) Sosnick, T. R.; Mayne, L.; Hiller, R.; Englander, S. W. *Nat. Struct. Biol.* **1994**, *1*, 149−156.
(77) Hampsey, D. M.; Das, G.; Sherman, F. *J. Biol. Chem.* **1986**, *261*, 3259−3271.
(78) Lan, W.; Wang, Z.; Yang, Z.; Zhu, J.; Ying, T.; Jiang, X.; Zhang, X.; Wu, H.; Liu, M.; Tan, X.; Cao, C.; Huang, Z. X. *PLoS One* **2011**, *6*, e27219.
(79) Louie, G. V.; Hutcheon, W. L.; Brayer, G. D. *J. Mol. Biol.* **1988**, *199*, 295−314.
(80) Wu, L. C.; Laub, P. B.; Elove, G. A.; Carey, J.; Roder, H. *Biochemistry* **1993**, *32*, 10271−10276.
(81) Berghuis, A. M.; Brayer, G. D. *J. Mol. Biol.* **1992**, *223*, 959−976.

DOI: 10.1021/acs.analchem.7b00844
Anal. Chem. 2017, 89, 8757−8765